

BLENDING OF CEPHEIDS IN M33

JOY M. CHAVEZ¹, LUCAS M. MACRI & ANNE PELLERIN²

George P. and Cynthia Woods Mitchell Institute in Fundamental Physics and Astronomy,
Department of Physics and Astronomy, Texas A&M University, 4242 TAMU, College Station, TX 77843-4242

Accepted for publication in the Astronomical Journal

ABSTRACT

A precise and accurate determination of the Hubble constant based on Cepheid variables requires proper characterization of many sources of systematic error. One of these is stellar blending, which biases the measured fluxes of Cepheids and the resulting distance estimates. We study the blending of 149 Cepheid variables in M33 by matching archival *Hubble Space Telescope* data with images obtained at the WIYN 3.5-m telescope, which differ by a factor of 10 in angular resolution.

We find that $55 \pm 4\%$ of the Cepheids have no detectable nearby companions that could bias the WIYN *V*-band photometry, while the fraction of Cepheids affected below the 10% level is $73 \pm 4\%$. The corresponding values for the *I* band are $60 \pm 4\%$ and $72 \pm 4\%$, respectively. We find no statistically significant difference in blending statistics as a function of period or surface brightness. Additionally, we report all the detected companions within $2''$ of the Cepheids (equivalent to 9 pc at the distance of M33) which may be used to derive empirical blending corrections for Cepheids at larger distances.

Subject headings: Cepheid Variables; Galaxies: Individual (M33)

1. INTRODUCTION

An accurate and precise measurement of the Hubble constant at the few-percent level imposes significant constraints on the equation of state of dark energy and other cosmologically relevant parameters (Komatsu et al. 2011). The next generation of surveys aimed at improving our understanding of dark energy will benefit from an even tighter constraint on H_0 (Weinberg et al. 2012) than the present bounds of 3.4% (Riess et al. 2011).

Cosmological applications of the Extragalactic Distance Scale (Freedman & Madore 2010) primarily rely on the Period-Luminosity relation of Cepheid variables (hereafter the “Leavitt law”, Leavitt & Pickering 1912) as the primary distance indicator. The upcoming *Gaia* mission (Prusti 2011) is expected to deliver a sub-percent calibration of the Leavitt law in the Milky Way (Windmark et al. 2011), which could in turn enable a 1% measurement of H_0 if all sources of systematic error are properly accounted for.

One of these sources of systematic error occurs when two or more neighboring (but not necessarily physically associated) stars fall within the same resolution element of an instrument and cannot be fit with separate point-spread functions (PSFs). This effect is commonly referred to as *blending* and it is different from *crowding* or confusion noise, which results in improper PSF fitting and/or inaccurate background subtraction due to a very high stellar density. An extreme example of blending in the absence of crowding is a Cepheid in a binary system located in a low-surface brightness environment. Blending will bias the measured flux of a Cepheid towards larger values, shifting the Leavitt law to brighter magnitudes and leading to systematically shorter dis-

tances and larger values of H_0 . Extreme blends can be readily identified by their effects on Cepheid colors and/or amplitude ratios and such tests are routinely carried out (Pellerin & Macri 2011; Scowcroft et al. 2009; Macri et al. 2006). However, low-level blends are unlikely to be identified by such cuts and may affect studies of the metallicity dependence of the Leavitt law (another source of systematic uncertainty) since they could mimic the photometric changes expected from differences in chemical abundances.

The Local Group galaxy M33 is a good testbed for studies of Cepheid systematics thanks to its relative proximity ($D = 895 - 965$ kpc, Bonanos et al. 2006; Pellerin & Macri 2011), moderate inclination angle ($i = 55^\circ$, Ho et al. 1997) and recent episodes of star formation which have resulted in large numbers of Cepheids throughout its disk (Hartman et al. 2006; Pellerin & Macri 2011). Scowcroft et al. (2009) used M33 Cepheids to study the “metallicity effect” of the Leavitt law, motivated by the large abundance gradient inferred from H II regions (Zaritsky et al. 1994; Magrini et al. 2007, 2010). However other studies (Urbaneja et al. 2005; Bresolin et al. 2010; Bresolin 2011) have determined a much shallower abundance gradient, which would make the metallicity effect considerably harder to measure.

The disk of M33 has been extensively imaged by the Hubble Space Telescope (HST) using the Wide-Field and Planetary Camera 2 (WFPC2) and the Advanced Camera for Surveys (ACS). The angular resolution of HST at optical wavelengths is 10-15 times better than the seeing at a good site on the surface of the Earth. Thus, a comparison of HST and ground-based images of the same Cepheids in M33 can yield useful insights into the nature of blending for more distant galaxies observed only with Hubble.

Previous studies of the influence of blends on the Cepheid Distance Scale, based on comparisons between ground-based and HST images of nearby galaxies were

¹ Current address: Gemini Observatory, Northern Operations Center, Hilo, HI, 96720. jchavez@gemini.edu

² Current address: Department of Physics, Mount Allison University, Sackville, NB E4L 1E6, Canada.

TABLE 1
HST OBSERVATIONS OF M33 USED IN THIS STUDY

Field Name	RA (J2000, deg)	Dec	Camera	Filters		Exp. time (s)		Prop. #	N Ceph.	Comments
				#1	#2	#1	#2			
b4w	23.6384	30.7818	WFPC2	555	814	400	400	5237	3	16 in P07
d2a	23.4066	30.8111	ACS	606	814	10414	20828	9873	7	U49 in S06
d4w	23.4519	30.7977	WFPC2	555	814	4800	5200	5914	5	U49 in K02
fla	23.6108	30.6291	ACS	606	814	10414	20828	9873	6	M9 in S06
flw	23.6388	30.6393	WFPC2	555	814	4800	5200	5914	1	2 in C01
glw	23.5049	30.6843	WFPC2	555	814	4800	5200	5914	3	R14 in K02
g2w	23.5185	30.6446	WFPC2	555	814	4800	5200	5914	13	10 in C01
g6w	23.4670	30.6671	WFPC2	555	814	1600	1200	5464	2	
gbw	23.4753	30.6373	WFPC2	555	814	2240	2120	6640	2	WW1 in C99
gdw	23.5209	30.6349	WFPC2	606	814	340	400	8059	2	
gew	23.4963	30.6280	WFPC2	606	814	1600	360	8059	5	also prop. #8805
h1w	23.4030	30.7095	WFPC2	606	814	8800	17600	9873	4	
h4a	23.4178	30.6439	ACS	606	814	2160	2160	10190	6	F1 in S09
h5a	23.3644	30.6539	ACS	606	814	2400	2500	10190	7	F2 in S09
j1w	23.5654	30.5517	WFPC2	606	814	1600	360	8059	2	also prop. #8805
j2a	23.4581	30.5973	ACS	606	814	6380	6624	10190	8	innermost in W09; D1 in S09
j2w	23.5308	30.5654	WFPC2	606	814	300	700	8059	2	
j4a	23.5010	30.5487	ACS	606	814	2400	2500	10190	5	F3 in S09
j5w	23.4733	30.6000	WFPC2	555	814	2240	2120	6640	2	15 in C01
jaw	23.4735	30.5632	WFPC2	555	814	2240	2080	6640	2	17 in C01
jbw	23.4523	30.5314	WFPC2	555	814	2240	2080	6640	4	
jcw	23.4697	30.5199	WFPC2	555	814	2240	2080	6640	1	
l1a	23.5497	30.4560	ACS	606	814	2160	2160	10190	1	F5 in S09
m1w	23.3728	30.6106	WFPC2	555	814	520	460	6431	10	
m3w	23.3535	30.5758	WFPC2	606	814	1600	360	8059	10	also prop. #8805
m4w	23.3179	30.5566	WFPC2	606	814	240	400	8059	4	
m5a	23.4161	30.4834	ACS	606	814	21260	26420	10190	4	D2 in S09, 26 in C01
m6a	23.3592	30.5109	ACS	606	814	2160	2160	10190	15	F4 in S09
n3a	23.2727	30.4538	ACS	606	814	2400	2500	10190	4	F6 in S09
q1a	23.3348	30.3706	ACS	606	814	21260	26420	10190	6	D3 in S09
q2a	23.3068	30.3919	ACS	606	814	2160	2160	10190	3	3rd outermost in W09; F7 in S09
q2w	23.3645	30.3742	WFPC2	555	814	4800	5200	5914	1	9 in C01; C38 in K02

NOTE. — C99: Chandar et al. (1999); C01: Chandar et al. (2001); K02: Kim et al. (2002); P07: Park & Lee (2007); S06: Sarajedini et al. (2006); S09: San Roman et al. (2009); W09: Williams et al. (2009)

carried out by Mochejska et al. (2000) in M31, by Mochejska et al. (2001) in M33, and by Bresolin et al. (2005) in NGC 300. In the case of M33, Mochejska et al. (2001) used HST/WFPC2 images and the Cepheid sample of the DIRECT survey (Macri et al. 2001). During the intervening decade there have been numerous additional HST observations of M33 using both WFPC2 and the Advanced Camera for Surveys (ACS), which enable us to study more Cepheids than Mochejska et al. (2001) and, in the case of ACS, with greater depth and finer pixel scale. Furthermore, we rely on a new synoptic survey of M33 (Pellerin & Macri 2011) carried out at the WIYN 3.5-m telescope with more Cepheids and better angular resolution than the DIRECT catalog.

Pellerin & Macri (2011) carried out extensive simulations based on the M33 ACS images to quantify the photometric bias due to crowding in their ground-based photometry. Considering the range of magnitudes and surface brightnesses spanned by the M33 Cepheid sample, they found that crowding bias increased as a function of magnitude but did not exhibit a dependence on surface brightness. Our paper complements their study by quantifying the photometric bias due to blending for Cepheids in M33.

We describe in §2 the data used in this paper and the photometry we measured; §3 describes the method used to quantify the level of blending; we discuss the results in §4 and compare them to previous work in §5. Our concluding remarks and suggestions for future work can be found in §6.

2. DATA AND ANALYSIS

We based our analysis on the Cepheid sample published by the M33 Synoptic Stellar Survey (Pellerin & Macri 2011). We identify these variables in HST images and search for companions unresolved in the ground-based data. We calculate blending statistics based on these companions.

2.1. Cepheid Sample

Our analysis is based on the sample of Cepheids listed in Table 3 of Pellerin & Macri (2011). The ground-based observations and analysis are described in detail in that publication, which we briefly summarize here. Data from the DIRECT survey of M33 (Macri et al. 2001) were combined with new images obtained at the 3.5-m Wisconsin-Indiana-Yale-NOAO (WIYN) telescope with the Mini-Mosaic (MiniMo) camera to detect 563 Cepheids ranging in period from 2 to 110 days. The typical FWHM of the WIYN images was $0''.75$, sampled at a plate scale of $0''.28/\text{pix}$. The photometry and astrometry were calibrated using the catalogs of Massey et al. (2006).

2.2. HST Data

We queried the Hubble Legacy Archive (HLA) and the Mikulski Archive for Space Telescopes (MAST)³

³ The HLA and MAST are operated by the Space Telescope Science Institute (STScI).

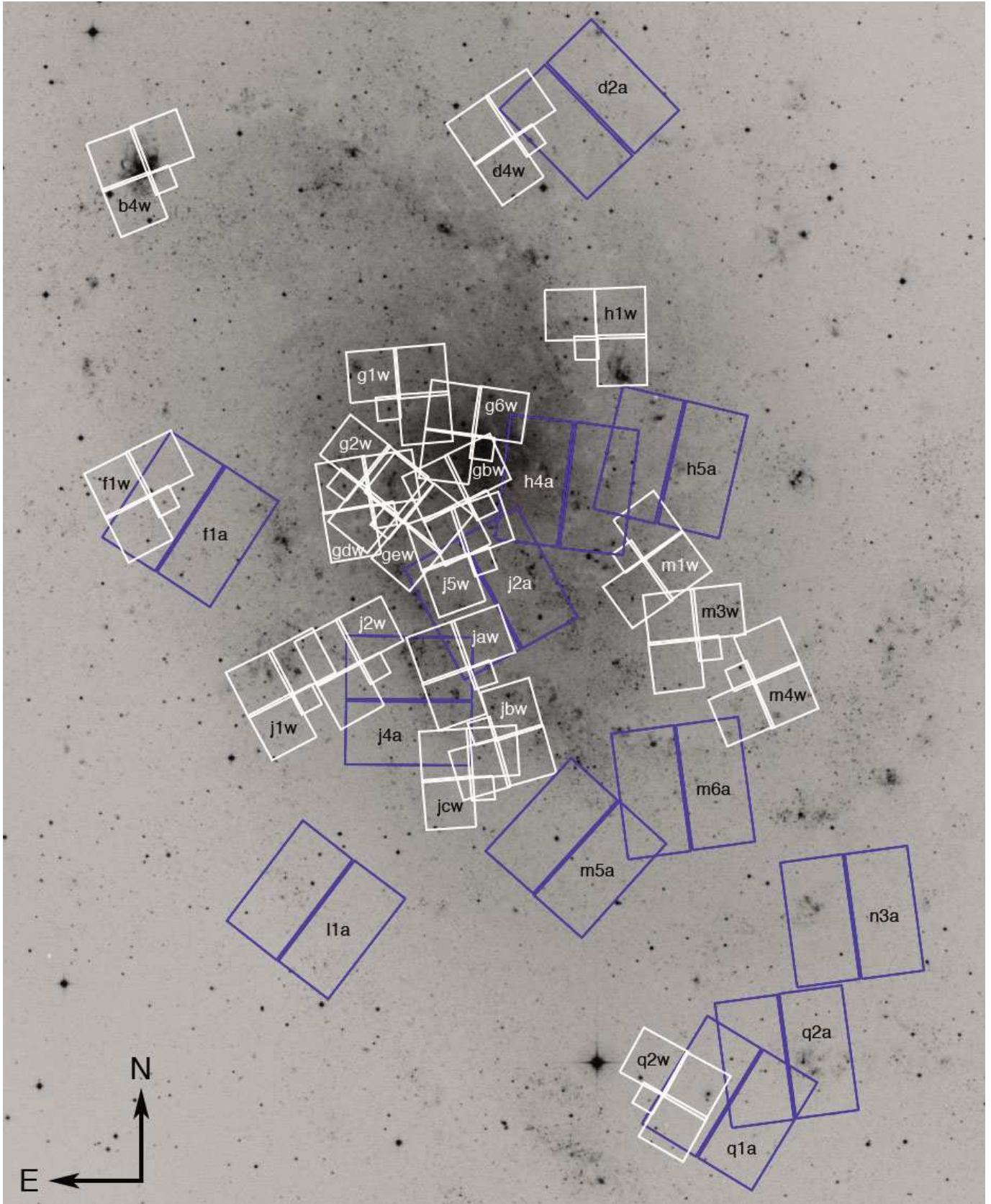


FIG. 1.— Footprints of the HST fields used in this study overlaid on a DPOSS-II image of M33. The blue rectangles are from ACS, and the white boxes are from WFPC2. The field label names end in 'a' for ACS, and 'w' for WFPC2.

for HST images of M33 obtained with either WFPC2 or ACS which had overlap with the WIYN images of Pellerin & Macri (2011). We selected observations with multiple exposures to allow for cosmic-ray removal. We also required a minimum of 100 s of total exposure time, to ensure a depth that would enable the detection of faint companions around the Cepheids. We further restricted our study to fields that were imaged in V (HST filters F555W or F606W) and I (HST filter F814W).

The HST fields contained 149 ($\sim 25\%$) of the Cepheids listed in Pellerin & Macri (2011). The locations of these fields are shown in Figure 1 and listed in Table 1. The table also contains references to previously-published analyses of the data. Except for two ACS fields, all images were acquired on a single epoch and we therefore only have imaging of the Cepheids at a random phase within their pulsation cycle.

The ACS images were reprocessed through the MAST On-The-Fly-Recalibration pipeline to apply the most up-to-date calibrations, while the WFPC2 images had already been reprocessed using the final set of calibration frames in mid 2009 by STScI (Gonzaga et al. 2010). We downloaded the reprocessed images and used MultiDrizzle (Koekemoer et al. 2002) to remove cosmic rays, correct for geometric distortions in the cameras, and co-add multiple observations into master images.

2.3. Photometry and Cepheid Search

We performed point-spread function (PSF) photometry using DAOPHOT and ALLSTAR (Stetson 1987). We derived model PSFs using grids of artificial stars created with TinyTim (Krist & Hook 2004) for the appropriate bandpasses, cameras and CCDs. We ran the FIND algorithm twice on each image, removing all stars found on the first iteration before proceeding to the second one. This increased the detection efficiency of faint stars, such as possible companions of a Cepheid. ALLSTAR was run one final time on the merged star list. Based on the observed luminosity functions, the photometry is complete to $V \sim 25.5$, $I \sim 24.7$ and $V \sim 24.3$, $I \sim 23$ mag for ACS and WFPC2, respectively.

Instrumental magnitudes were converted to the HST VEGAMAG system using the equations listed in Appendix D of Sirianni et al. (2005) and the coefficients listed in Table 10 of Sirianni et al. (2005) and Table 2 of Dolphin (2009) for ACS and WFPC2, respectively.

Given the vastly different resolution and depth of the HST and WIYN images, the former had significantly larger stellar densities. Furthermore, the astrometric solution provided by the automated STScI pipeline is only accurate to a few arcseconds (Koekemoer et al. 2005). We obtained a rough initial match between HST and WIYN images using the brightest few hundred stars in common. Once the gross astrometric offset had been removed, we matched the complete star lists using DAOMATCH and DAOMASTER (Stetson 1993) and refined the astrometric solution of the HST images. Cepheids were then selected based on the coordinates tabulated by Pellerin & Macri (2011). We visually inspected every Cepheid to ensure the star in the HST frame was indeed a match to the same star in WIYN image. This process helped to identify and correct a few erroneous matches where a faint star close to the Cepheid was originally

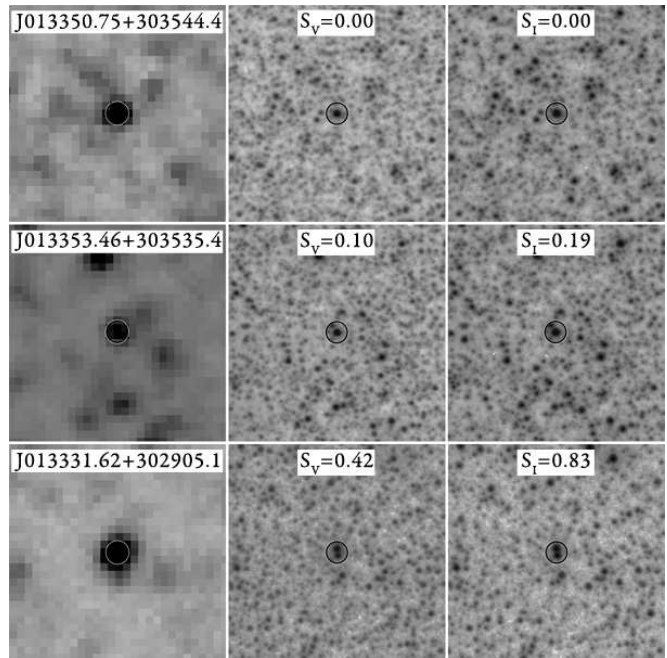


FIG. 2.— Comparison of HST and WIYN images of three Cepheids in M33, illustrating different blending values. Left column: WIYN V images; center column: HST V images; right column: HST I images. Panels are $8''$ on a side and the black circles are $0.75''$ in diameter, equal to the WIYN FWHM.

identified as the variable in the HST frame. Lastly, we estimated the disk surface brightness by averaging the background flux values reported by ALLSTAR for stars within $7''$ of each Cepheid.

3. BLENDING CALCULATION

We quantify the level of blending following the prescription of Mochejska et al. (2000),

$$S_F = \sum (f_i) / f_C \quad (1)$$

where S_F is the total flux contribution from the companions relative to the Cepheid in filter F , f_i is the flux of an individual companion star located within the critical radius and f_C is the flux of the Cepheid.

We calculated the values of S separately for V and I , using a critical radius of $0''.375$ which is the average value of the half-width at half-maximum (HWHM) of the WIYN PSF. We only include companions that contribute 4% or more of the flux of a Cepheid in order to provide a conservative estimate of the blending value. This cut-off was adopted by Mochejska et al. (2000), although Mochejska et al. (2001) raised it to 6%. In practice, stars with $f_i \sim 0.05 f_C$ (or $\Delta \text{mag} \sim 3.25$) are near the completeness limit of the ACS images relative to the faintest, shortest-period Cepheids, which have $V \sim 22.5$, $I \sim 21.5$ mag.

In the case of Cepheids present in both ACS and WFPC2 images, we calculated blending values using the ACS data given its finer spatial sampling and increased depth. In the case of Cepheids present in multiple fields obtained with the same camera, we gave preference to the image with the deepest exposure time. If the exposures were of similar depth, we averaged the Cepheid magnitudes and the S values.

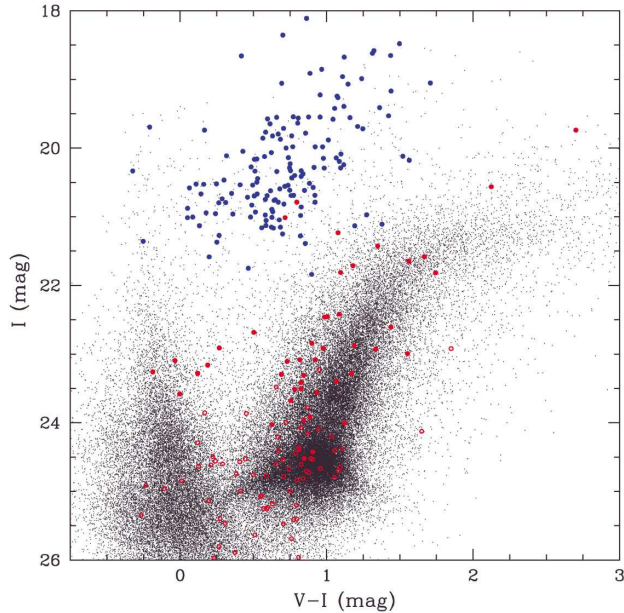


FIG. 3.— Color-magnitude diagram of M33 Cepheids (in blue) and companions within $0''.375$ (in red), contributing more (filled) or less (open) than 4% of the Cepheid flux. Black dots are used to plot 3.5% of the stars detected in the ACS frames with $I < 26$ mag.

Figure 2 shows a comparison of HST and WIYN images for three Cepheids with different values of S . Each panel is $8''$ on a side, centered on a Cepheid. Circles with radii of $0''.375$ (typical WIYN HWHM) are drawn around the variables. The Cepheids were chosen to show the range of blending values, from $S_F = 0$ (top row) to $S_F \sim 0.6$ (bottom row). The left column shows the WIYN V images, while the center and right columns show the V and I HST images.

The photometry and blending values are listed in Table 2. For each Cepheid, we list the ID and period from Pellerin & Macri (2011), the V magnitude and its uncertainty, the value of S_V and its uncertainty, and the corresponding information for the I band. Additionally, we tabulate the V and I surface brightness values and the designations of the WIYN and HST fields where each Cepheid is located. The uncertainties in S_F values are calculated by propagating the reported ALLSTAR photometric uncertainties through Eqn. 1. HST field codes are based on the field name listed in the first column of Table 1, followed by a letter to identify the camera (‘a’ for ACS, ‘w’ for WFPC2).

Figure 3 shows a color-magnitude diagram of the Cepheids and all companions located within the critical radius. As a reference, we also plot 3.5% of all the stars with $I < 26$ mag detected in the V and I ACS frames. The companions span a broad range of colors and magnitudes, but most are associated with the red giant branch and the red clump. These findings are not directly applicable to all Cepheid hosts, since different star-formation histories will alter the relative contributions of the upper main-sequence and the red giant branch.

We used the HST star lists obtained in §2.3 to tabulate all companions within a $2''$ radius of each Cepheid, presented in Table 3. Companions are labeled using the Cepheid ID from Table 2 and are numbered in increasing

order of radial distance from the variable. We list the x -, y - and radial distance from the Cepheid (in arcseconds), the V magnitude and uncertainty, and the I magnitude and uncertainty. Some companions were only detected in one band.

This extended dataset can be used for a variety of future studies. For example, comparisons of HST data with ground-based observations of M33 at different angular resolutions can be easily carried out by selecting the appropriate critical radius. Likewise, the sensitivity of blending values to the faint-companion cutoff limit can be explored. Lastly, suitable scaling of fluxes and angular separations can yield simulated HST images of Cepheids in similar environments out to $D \sim 35$ Mpc, at which point $2''$ at the distance of M33 would be equivalent to the angular resolution of HST in the V band.

4. RESULTS

We find mean blending values of $S_V = 0.096 \pm 0.015$ and $S_I = 0.083 \pm 0.013$ and median values of zero for both bands. Figure 4 shows cumulative distributions of blending values, while Figures 5 and 6 show the distribution of blending values as a function of period and surface brightness, respectively. Table 4 lists the fractions of Cepheids which meet several blending criteria as a function of period and surface brightness. We calculated the uncertainty in each fraction using the binomial distribution approximation,

$$\sigma(f) = \sqrt{f(1-f)/N} \quad (2)$$

where f is the fraction value and N is the number of Cepheids meeting a particular set of criteria. We cross-checked the validity of this approximation by performing 100,000 bootstrap resamplings with replacement, which yielded the same uncertainties. Lastly, we tested the sensitivity to outliers in the distributions by performing the same number of jackknife resamplings, keeping 90% of the original sample. The derived fractions remained stable at the 2% level.

The fraction of Cepheids with no blending is marginally lower ($\sim 1\sigma$) for Cepheids with $P < 10$ d than for ones with $P > 10$ d. Such a trend might be expected because the shorter-period, less luminous Cepheids can be affected (at a fixed flux ratio) by a larger fraction of disk stars. However, the difference vanishes when comparing the statistics of Cepheids affected at the 10% level. There is no significant difference in the statistics of Cepheids located in areas with “high” or “low” surface brightness.

We also examined the effect of blends on the color of the Cepheids by calculating the value of $S_V - S_I$ for all Cepheids with non-zero values of either S_V or S_I . The resulting histogram, presented in Figure 7, shows that most blends do not appreciably change the color of the Cepheids: $\langle S_V - S_I \rangle = 0.03 \pm 0.27$.

5. COMPARISON WITH PREVIOUS WORK

Mochejska et al. (2001) analyzed WFPC2 images of M33 Cepheids discovered by the DIRECT project. We recalculated our blending values using the parameters adopted in that paper: a critical radius of $0''.75$ and

TABLE 2
 CEPHEID PROPERTIES (ABRIDGED)

ID	P (d)	V (mag)	σ_V	S_V	σ_{S_V}	I (mag)	σ_I	S_I	σ_{S_I}	SB_V (mag/ \square'')	SB_I (mag/ \square'')	Field	
												HST	WIYN
J013332.36+302819.8	2.689	21.635	0.038	0.000	0.000	21.008	0.032	0.000	0.000	21.92	21.26	m5a	m0f
J013324.20+302248.9	2.695	21.620	0.038	0.073	0.005	21.369	0.029	0.155	0.008	21.51	20.96	q1a	m0m
J013316.88+302157.9	3.187	22.737	0.106	0.316	0.087	21.839	0.055	0.000	0.000	21.55	21.01	q1a	m0m
J013309.08+302354.6	3.260	22.215	0.067	0.000	0.000	21.750	0.043	0.000	0.000	21.94	21.39	q2a	m0m
J013329.48+303614.3	3.760	21.520	0.102	0.000	0.000	20.893	0.125	0.000	0.000	21.41	20.56	m1w	m0j
J013312.30+302355.7	4.053	21.457	0.072	0.089	0.041	20.787	0.062	0.000	0.000	21.87	21.33	q2a	m0m
J013322.10+303731.9	4.584	20.768	0.087	0.000	0.000	20.520	0.082	0.000	0.000	21.72	21.03	h5a	m0j
J013428.61+304820.7	4.634	22.243	0.059	0.000	0.000	21.389	0.085	0.000	0.000	21.89	20.45	b4w	m03
J013350.94+303117.4	4.767	21.559	0.060	0.158	0.015	20.927	0.035	0.564	0.025	21.33	20.46	jbw	m0e
J013320.60+303458.4	4.889	21.090	0.137	0.123	0.024	21.004	0.128	0.000	0.000	21.53	20.85	m3w	m0k
J013319.10+303305.6	4.933	21.445	0.048	0.000	0.000	20.931	0.068	0.000	0.000	21.30	20.78	m4w	m0k
J013307.46+302512.6	5.166	21.949	0.037	0.000	0.000	21.250	0.033	0.000	0.000	21.90	21.37	q2a	m0m
J013328.77+303753.4	5.176	21.196	0.054	0.163	0.016	20.954	0.065	0.364	0.050	21.29	20.40	m1w	m0j
J013342.17+304841.0	5.177	21.321	0.102	0.040	0.005	20.961	0.047	0.063	0.003	21.76	21.14	d2a	m0b
J013341.39+304736.4	5.190	21.837	0.051	0.148	0.013	21.152	0.049	0.152	0.009	21.69	21.05	d2a	m0b
J013316.08+302051.8	5.204	21.642	0.065	0.000	0.000	21.055	0.058	0.000	0.000	21.48	20.91	q1a	m0n
J013405.98+303454.0	5.281	21.034	0.048	0.047	0.011	20.539	0.024	0.000	0.000	21.02	20.38	j2w	m0e
J013321.78+303234.9	5.282	21.685	0.298	0.398	0.119	20.858	0.038	0.000	0.000	21.31	20.78	m4w	m0k
J013308.37+302607.0	5.314	21.774	0.057	0.000	0.000	21.151	0.055	0.000	0.000	22.07	21.39	n3a	m0l
J013408.64+303754.7	5.316	21.287	0.058	0.000	0.000	20.693	0.089	0.110	0.021	21.08	20.20	g2w	m0d
J013325.71+302138.7	5.571	21.538	0.045	0.076	0.007	21.272	0.029	0.128	0.010	21.54	21.01	q1a	m0m
J013321.51+302132.0	5.683	21.555	0.066	0.074	0.015	20.974	0.037	0.092	0.018	21.54	21.00	q1a	m0m
J013332.14+303002.3	5.791	21.803	0.108	0.207	0.015	20.981	0.030	0.067	0.004	24.53	23.07	m6a	m0f
J013429.09+303735.1	5.828	21.782	0.034	0.157	0.007	21.584	0.074	0.170	0.014	21.81	21.14	fla	m05
J013425.11+303541.4	5.868	20.809	0.033	0.000	0.000	20.667	0.081	0.000	0.000	21.80	21.12	fla	m05
J013350.99+303156.4	5.889	21.403	0.091	0.254	0.061	20.762	0.113	0.417	0.146	21.14	20.25	jcw	m0e
J013407.94+303831.2	5.902	21.060	0.028	0.000	0.000	20.796	0.072	0.144	0.024	21.11	20.24	gdw	m0d
J013359.89+303800.0	5.997	21.204	0.057	0.000	0.000	20.698	0.065	0.000	0.000	20.52	19.83	gew	m0d
J013349.55+304743.7	6.010	21.718	0.031	0.000	0.000	21.161	0.078	0.000	0.000	21.39	20.53	d4w	m0b
J013333.08+304230.8	6.015	21.802	0.065	0.000	0.000	21.165	0.053	0.000	0.000	21.10	20.55	h1w	m0c
J013350.67+303445.9	6.031	21.063	0.064	0.235	0.016	21.013	0.034	0.612	0.021	21.20	20.51	j2a	m0e
J013325.62+303510.8	6.111	21.010	0.040	0.000	0.000	20.659	0.084	0.000	0.000	21.41	20.71	m3w	m0k
J013328.37+303730.9	6.116	21.238	0.057	0.000	0.000	20.621	0.069	0.000	0.000	21.30	20.39	m1w	m0j
J013353.70+303152.0	6.276	21.709	0.103	0.491	0.048	20.788	0.056	0.041	0.003	21.53	20.92	j4a	m0e
J013346.45+304740.5	6.333	21.272	0.065	0.100	0.015	20.557	0.085	0.000	0.000	21.31	20.45	d4w	m0b
J013401.87+304148.3	6.333	21.714	0.035	0.000	0.000	21.128	0.071	0.369	0.033	21.07	20.16	glw	m0c
J013400.58+303630.6	6.346	20.846	0.021	0.000	0.000	20.335	0.048	0.000	0.000	20.68	20.06	gew	m0d
J013351.82+303310.9	6.504	22.100	0.093	0.000	0.000	21.279	0.041	0.417	0.175	21.19	20.35	jaw	m0e
J013329.22+303136.0	6.530	21.020	0.049	0.000	0.000	20.496	0.042	0.000	0.000	22.88	22.26	m6a	m0k
J013315.71+303319.3	6.557	21.464	0.161	0.084	0.019	20.615	0.052	0.084	0.015	21.45	20.96	m4w	m0k

 TABLE 3
 STARS FOUND WITHIN $2''$ OF CEPHEID VARIABLES (ABRIDGED)

ID	Δx	Δy ($''$)	Δr	V	σ_V (mag)	I	σ_I
J013302.03+302553.4-c001	-0.112	0.010	0.112	24.021	0.434
J013302.03+302553.4-c002	-0.109	0.221	0.247	25.333	0.134	25.139	0.115
J013302.03+302553.4-c003	0.333	-0.132	0.358	26.490	0.091
J013302.03+302553.4-c004	-0.306	0.260	0.402	26.442	0.190	25.226	0.338
J013302.03+302553.4-c005	0.375	0.203	0.427	25.891	0.126	24.051	0.085
J013302.03+302553.4-c006	0.454	-0.033	0.455	25.141	0.119	24.446	0.099
J013302.03+302553.4-c007	0.047	0.567	0.569	27.163	0.113
J013302.03+302553.4-c008	0.128	0.652	0.664	27.007	0.081
J013302.03+302553.4-c009	0.109	-0.743	0.751	26.728	0.069	26.302	0.096
J013302.03+302553.4-c010	-0.790	-0.128	0.800	22.802	0.071	21.326	0.048
J013302.03+302553.4-c011	-0.787	-0.223	0.818	25.424	0.247
J013302.03+302553.4-c012	0.069	0.870	0.872	27.152	0.145
J013302.03+302553.4-c013	0.877	0.051	0.878	27.355	0.143
J013302.03+302553.4-c014	0.855	-0.279	0.899	26.387	0.133	25.761	0.105
J013302.03+302553.4-c015	-0.853	0.323	0.912	27.702	0.143
J013302.03+302553.4-c016	0.628	0.738	0.969	25.763	0.101	25.536	0.100
J013302.03+302553.4-c017	0.289	-0.941	0.985	26.810	0.114	26.077	0.119
J013302.03+302553.4-c018	-1.016	0.074	1.019	24.672	0.065	23.880	0.071
J013302.03+302553.4-c019	0.588	0.858	1.040	27.127	0.113
J013302.03+302553.4-c020	-0.842	0.663	1.071	26.431	0.096	26.194	0.111
J013302.03+302553.4-c021	0.512	-0.966	1.093	27.062	0.111	26.481	0.094

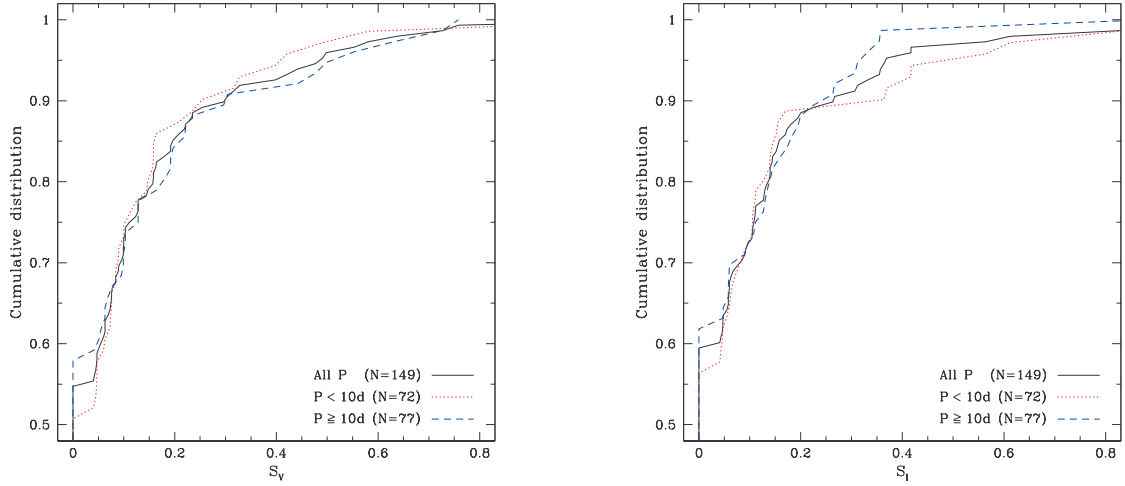


FIG. 4.— Cumulative distributions of the blending values in the V and I bands (right and left panels, respectively). The solid lines represent the entire Cepheid sample while the dotted and dashed lines denote the short- and long-period ($P \leq 10$, $P > 10$ d) Cepheids, respectively.

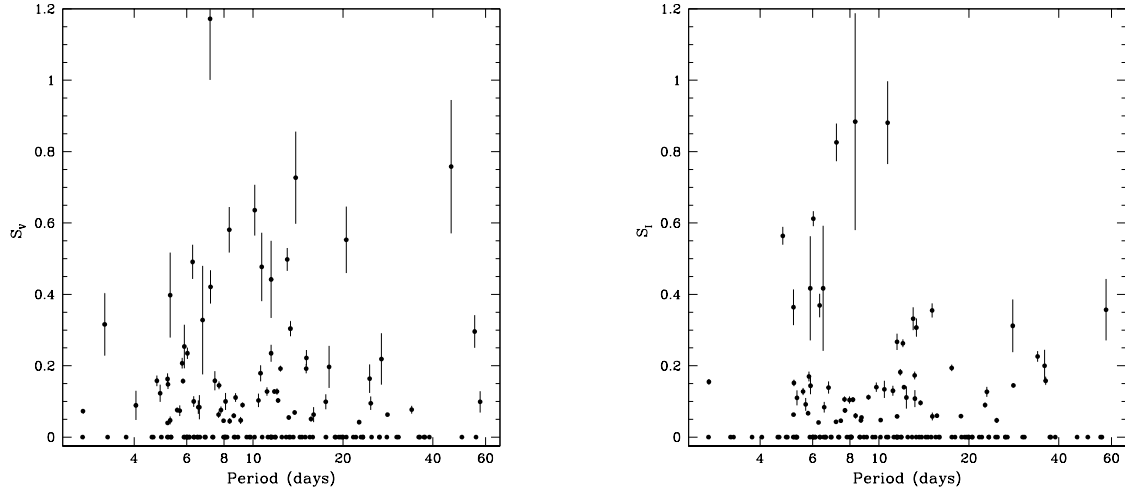


FIG. 5.— Blending values as a function of the period of the Cepheid.

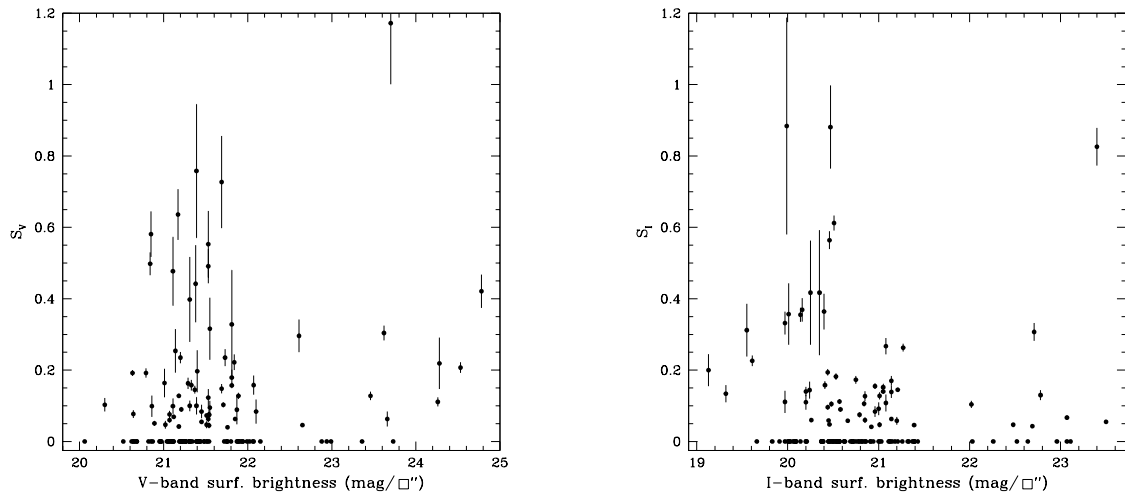


FIG. 6.— Blending values as a function of the sky background.

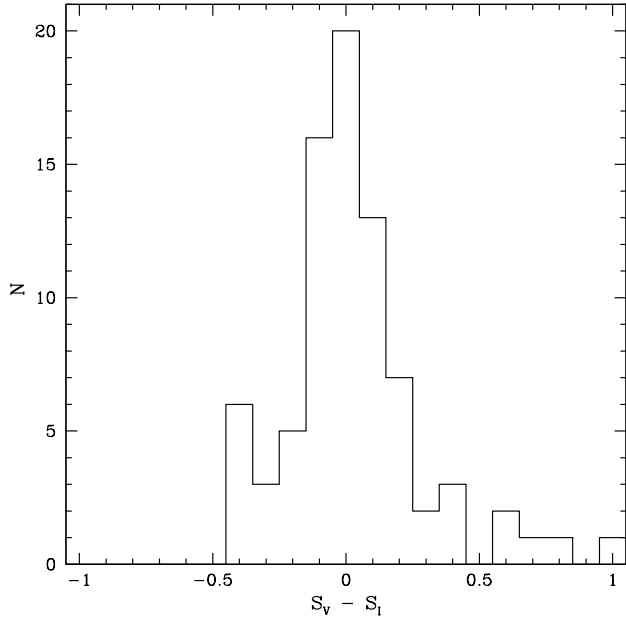


FIG. 7.— Distribution of the “color” of the companions relative to their Cepheid.

TABLE 4
BLENDING STATISTICS

Blending level	Sub-sample	N	Blending criteria	
			CMP12 %	M01 %
$S_V = 0$	all	149	55 ± 4	30 ± 4
$S_V = 0$	$P < 10d$	72	50 ± 6	22 ± 5
$S_V = 0$	$P > 10d$	77	57 ± 6	35 ± 5
$S_V = 0$	$\Sigma_V < 21.4$	71	61 ± 6	30 ± 5
$S_V = 0$	$\Sigma_V > 21.4$	78	47 ± 6	28 ± 5
$S_V < 0.1$	all	149	73 ± 4	45 ± 4
$S_V < 0.1$	$P < 10d$	72	74 ± 5	43 ± 6
$S_V < 0.1$	$P > 10d$	77	70 ± 5	46 ± 6
$S_V < 0.1$	$\Sigma_V < 21.4$	71	76 ± 5	44 ± 6
$S_V < 0.1$	$\Sigma_V > 21.4$	78	68 ± 5	45 ± 6
$S_I = 0$	all	149	60 ± 4	30 ± 4
$S_I = 0$	$P < 10d$	72	56 ± 6	19 ± 4
$S_I = 0$	$P > 10d$	77	61 ± 6	38 ± 6
$S_I = 0$	$\Sigma_I < 20.7$	74	60 ± 6	24 ± 5
$S_I = 0$	$\Sigma_I > 20.7$	75	57 ± 6	33 ± 5
$S_I < 0.1$	all	149	72 ± 4	41 ± 4
$S_I < 0.1$	$P < 10d$	72	71 ± 5	33 ± 5
$S_I < 0.1$	$P > 10d$	77	71 ± 5	47 ± 5
$S_I < 0.1$	$\Sigma_I < 20.7$	74	66 ± 5	32 ± 5
$S_I < 0.1$	$\Sigma_I > 20.7$	75	76 ± 5	48 ± 5

NOTE. — CMP12: this work; M01: Mochejska et al. (2001)

a companion flux cutoff of 6%. The results are tabulated in the rightmost column of Table 4. We also compared the individual blending values measured for 33 variables in common in V and I . As seen in Figure 8, there is good agreement with $\langle \Delta S_F \rangle = -0.02 \pm 0.13$.

The statistics derived using the criteria of Mochejska et al. (2001) are in excellent agreement with the values presented in their paper. For example, the fraction of Cepheids with $S_V < 0.1$ becomes $45 \pm 4\%$, compared to their value of $\sim 43 \pm 5\%$ (inferred from their Fig. 4 and Table 2). We also obtain identical values

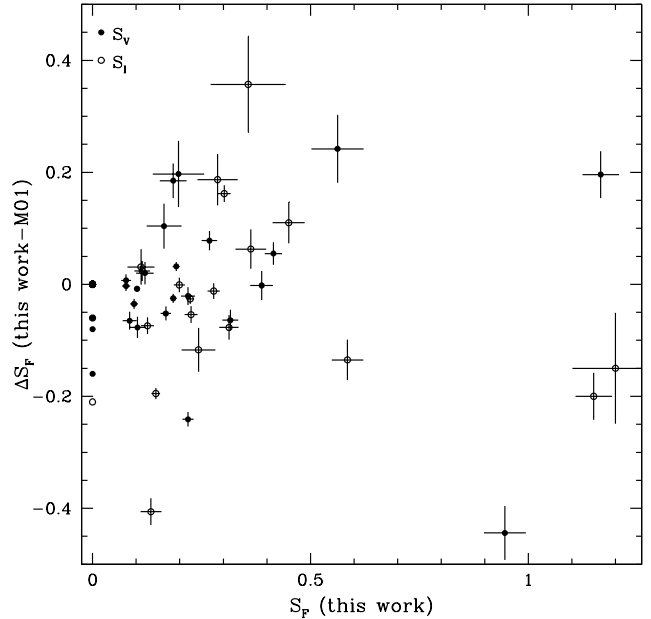


FIG. 8.— Comparison of blending values for Cepheids in common (found in WFPC2 images) with Mochejska et al. (2001); our analysis was redone using their criteria. Filled (open) circles are used to plot the blending values in the V (I) filter.

for the mean and median blending levels ($24 \pm 3\%$ and 13%) and reproduce the difference in blending statistics for “short” and “long” period Cepheids. Clearly, the differences between the two sets of values presented in Table 4 are due to the $2\times$ smaller critical radius adopted in our study, and emphasize the importance of angular resolution.

We also compared the disk surface brightness values we derived with those determined by (Mochejska et al. 2001) and found agreement at the level of $0.2 \text{ mag}/\square''$. We note that our surface brightness calculation is based on the average background level of the HST images within $7''$ of the Cepheid, while Mochejska et al. (2001) used the DIRECT ground-based images to calculate the sky in an annulus about $6''$ from the Cepheid. Regardless of the method used to measure the background or the blending criteria adopted, there is little (if any) correlation between blending fraction and surface brightness for the range of values considered here.

Bresolin et al. (2005) calculated blending statistics for a small sample of 16 Cepheids in NGC 300 using HST/ACS images. They found a median value of 0% and an average value of 7%. Our results are consistent with their findings.

6. CONCLUDING REMARKS

We have presented a survey of Cepheids in M33 and their companions within $2''$, as resolved by HST with the ACS and WFPC2 cameras. We calculated the flux contribution of the companions when they are blended (unresolved) in ground-based images with a seeing of $0''.75$. We find that more than half of the Cepheids in our sample exhibit no blending at V and I , regardless of period or surface brightness. The majority of companion stars are located in the red giant branch and do not significantly alter the derived color of the Cepheids.

We plan to combine the ground-based photometry of Pellerin & Macri (2011) with the blending values derived in this paper to investigate possible biases in the determination of distance moduli and “metallicity corrections” when using samples that lack such higher-resolution imaging. Additionally, our compilation of companions may be useful to derive empirical photometric bias corrections for Cepheids in more distant galaxies studied with the *Hubble Space Telescope*, provided the variables are located in similar environments to the M33 sample.

JMC acknowledges support by the Department of Education through the GAANN Fellowship Program. AP and LMM acknowledge financial support through a

Texas A&M University faculty startup fund. We thank Profs. Jianhua Huang and Lan Zhou for useful discussions on statistical techniques and the referee, Dr. Barry Madore, for his very helpful comments.

Based on observations made with the NASA/ESA Hubble Space Telescope and obtained using the Mikulski Archive for Space Telescopes and the Hubble Legacy Archive (HLA) at STScI. STScI is operated by the Association of Universities for Research in Astronomy, Inc. under NASA contract NAS 5-26555. The HLA is a collaboration between STScI/NASA, the Space Telescope European Coordinating Facility (ST-ECF/ESA) and the Canadian Astronomy Data Centre (CADC/NRC/CSA).

Facilities: HST (WFPC2, ACS), WIYN (MiniMo)

REFERENCES

- Bonanos, A. Z., Stanek, K. Z., Kudritzki, R. P., Macri, L. M., Sasselov, D. D., Kaluzny, J., Stetson, P. B., Bersier, D., Bresolin, F., Matheson, T., Mochejska, B. J., Przybilla, N., Szentgyorgyi, A. H., Tonry, J., & Torres, G. 2006, *ApJ*, 652, 313
- Bresolin, F. 2011, *ApJ*, 730, 129
- Bresolin, F., Pietrzyński, G., Gieren, W., & Kudritzki, R.-P. 2005, *ApJ*, 634, 1020
- Bresolin, F., Stasińska, G., Vilchez, J. M., Simon, J. D., & Rosolowsky, E. 2010, *MNRAS*, 404, 1679
- Chandar, R., Bianchi, L., & Ford, H. C. 1999, *ApJS*, 122, 431
- . 2001, *A&A*, 366, 498
- Dolphin, A. E. 2009, *PASP*, 121, 655
- Freedman, W. L. & Madore, B. F. 2010, *ARA&A*, 48, 673
- Gonzaga, S., Biretta, J., & et al. 2010, *HST WFPC2 Data Handbook* (Baltimore: STScI)
- Hartman, J. D., Bersier, D., Stanek, K. Z., Beaulieu, J.-P., Kaluzny, J., Marquette, J.-B., Stetson, P. B., & Schwarzenberg-Czerny, A. 2006, *MNRAS*, 371, 1405
- Ho, L. C., Filippenko, A. V., & Sargent, W. L. W. 1997, *ApJS*, 112, 315
- Kim, M., Kim, E., Lee, M. G., Sarajedini, A., & Geisler, D. 2002, *AJ*, 123, 244
- Koekemoer, A. M., Fruchter, A. S., Hook, R. N., & Hack, W. 2002, in *The 2002 HST Calibration Workshop : Hubble after the Installation of the ACS and the NICMOS Cooling System*, ed. S. Arribas, A. Koekemoer, & B. Whitmore, 337–+
- Koekemoer, A. M., McLean, B., McMaster, M., & Jenkner, H. 2005, *Demonstration of a Significant Improvement in the Astrometric Accuracy of HST Data*, Tech. rep., Space Telescope Science Institute
- Komatsu, E., Smith, K. M., Dunkley, J., Bennett, C. L., Gold, B., Hinshaw, G., Jarosik, N., Larson, D., Nolte, M. R., Page, L., Spergel, D. N., Halpern, M., Hill, R. S., Kogut, A., Limon, M., Meyer, S. S., Odegard, N., Tucker, G. S., Weiland, J. L., Wollack, E., & Wright, E. L. 2011, *ApJS*, 192, 18
- Krist, J. & Hook, R. 2004, *The Tiny Tim User’s Guide* (Baltimore: STScI)
- Leavitt, H. S. & Pickering, E. C. 1912, *Harvard College Observatory Circular*, 173, 1
- Macri, L. M., Stanek, K. Z., Bersier, D., Greenhill, L. J., & Reid, M. J. 2006, *ApJ*, 652, 1133
- Macri, L. M., Stanek, K. Z., Sasselov, D. D., Krockenberger, M., & Kaluzny, J. 2001, *AJ*, 121, 870
- Magrini, L., Stanghellini, L., Corbelli, E., Galli, D., & Villaver, E. 2010, *A&A*, 512, A63+
- Magrini, L., Vilchez, J. M., Mampaso, A., Corradi, R. L. M., & Leisy, P. 2007, *A&A*, 470, 865
- Massey, P., Olsen, K. A. G., Hodge, P. W., Strong, S. B., Jacoby, G. H., Schlingman, W., & Smith, R. C. 2006, *AJ*, 131, 2478
- Mochejska, B. J., Macri, L. M., Sasselov, D. D., & Stanek, K. Z. 2000, *AJ*, 120, 810
- . 2001, *ArXiv Astrophysics e-prints*, astro-ph/0103440
- Park, W.-K. & Lee, M. G. 2007, *AJ*, 134, 2168
- Pellerin, A. & Macri, L. M. 2011, *ApJS*, 193, 26
- Prusti, T. 2011, in *EAS Publications Series*, Vol. 45, *EAS Publications Series*, 9–14
- Riess, A. G., Macri, L., Casertano, S., Lampeitl, H., Ferguson, H. C., Filippenko, A. V., Jha, S. W., Li, W., & Chornock, R. 2011, *ApJ*, 730, 119
- San Roman, I., Sarajedini, A., Garnett, D. R., & Holtzman, J. A. 2009, *ApJ*, 699, 839
- Sarajedini, A., Barker, M. K., Geisler, D., Harding, P., & Schommer, R. 2006, *AJ*, 132, 1361
- Scowcroft, V., Bersier, D., Mould, J. R., & Wood, P. R. 2009, *MNRAS*, 396, 1287
- Sirianni, M., Jee, M. J., Benítez, N., Blakeslee, J. P., Martel, A. R., Meurer, G., Clampin, M., De Marchi, G., Ford, H. C., Gilliland, R., Hartig, G. F., Illingworth, G. D., Mack, J., & McCann, W. J. 2005, *PASP*, 117, 1049
- Stetson, P. B. 1987, *PASP*, 99, 191
- Stetson, P. B. 1993, in *IAU Colloq. 136: Stellar Photometry - Current Techniques and Future Developments*, ed. C. J. Butler & I. Elliott, 291
- Urbaneja, M. A., Herrero, A., Kudritzki, R.-P., Najarro, F., Smartt, S. J., Puls, J., Lennon, D. J., & Corral, L. J. 2005, *ApJ*, 635, 311
- Weinberg, D. H., Mortonson, M. J., Eisenstein, D. J., Hirata, C., Riess, A. G., & Rozo, E. 2012, *Physics Reports*, in press
- Williams, B. F., Dalcanton, J. J., Dolphin, A. E., Holtzman, J., & Sarajedini, A. 2009, *ApJ*, 695, L15
- Windmark, F., Lindgren, L., & Hobbs, D. 2011, *A&A*, 530, A76
- Zaritsky, D., Kennicutt, Jr., R. C., & Huchra, J. P. 1994, *ApJ*, 420, 87